Generation of High Dynamic Range Illumination from a Single Image for the Enhancement of Undesirably Illuminated Images

Jae Sung Park*†, Nam Ik Cho*

*INMC, Department of Electrical and Computer Engineering, Seoul National University, Seoul, South Korea

jason79.park@ispl.snu.ac.kr, nicho@snu.ac.kr

†Visual Display Division, SAMSUNG Electronics Co. Ltd., Suwon, South Korea

Abstract—**This paper presents an algorithm that enhances undesirably illuminated images by generating and fusing multi-level illuminations from a single image. The input image is first decomposed into illumination and reflectance components by using an edge-preserving smoothing filter. Then the reflectance component is scaled up to improve the image details in bright areas. The illumination component is scaled up and down to generate several illumination images that correspond to certain camera exposure values different from the original. The virtual multi-exposure illuminations are blended into an enhanced illumination, where we also propose a method to generate appropriate weight maps for the tone fusion. Finally, an enhanced image is obtained by multiplying the equalized illumination and enhanced reflectance. Experiments show that the proposed algorithm produces visually pleasing output and also yields comparable objective results to the conventional enhancement methods, while requiring modest computational loads.**

Index Terms—**Image enhancement, Single image HDR, Illumination adjustment, Retinex filtering, Multi-exposure fusion, Tone fusion.**

I. INTRODUCTION

MANY kinds of image enhancement and restoration algorithms have been proposed for several decades to deal with so many kinds of image degradation [1, 2]. In this paper, we focus on the degradation due to undesirable lighting conditions, for example low light or backlight situations [3–7]. Images obtained under the low light conditions such as nighttime, underwater and medical images suffer from low contrast and low signal to noise ratio. Also, the details in bright or dark areas are often lost in backlight and/or non-uniform lighting situations, because the dynamic range of commercial cameras is not wide enough.

To improve the quality of degraded images captured in undesirable illumination conditions, a variety of image enhancement methods have been proposed. Many of the existing methods are based on the histogram equalization [3, 8–11], which attempt to expand the histogram of pixel values for boosting the details in near-saturated areas. On the other hand, image filtering-based methods have also been proposed in [4, 12–16], which exploit edge-preserving filters for the manipulation of decomposed image components or flash/non-flash image pairs. In addition, image enhancement algorithms based on Retinex filtering have been proposed in [5, 6, 17–19]. According to Retinex theory, color perception of human visual system (HVS) has a strong correlation with the reflectance of objects and the characteristics of illumination [17]. Hence, most of the Retinex-based approaches generally estimate the illumination component of the input, and then remove it from the input to retrieve the reflectance component. Then the illumination components are separately processed to obtain the enhanced images [5, 6]. However, the estimated illumination images often look unreasonable when the input is acquired in the under-exposure or over-exposure conditions. To alleviate this problem, there is also a more sophisticated method to estimate and/or refine the illuminations [7].

Recently, single image high dynamic range (HDR) imaging methods have been proposed for increasing the dynamic range of a single low dynamic range (LDR) image [5, 20, 21]. The original HDR imaging technique is to capture multiple images with different exposures, and produce larger bit depth images by combining them or produce tone-mapped-like images by adding them with appropriate weights [22, 23]. The main part of HDR imaging is to obtain multi-exposure images by using time-division or space-division multiple acquisition. The time-division acquisition is also called the bracketing, which is implemented in many of commercial cameras. This technique indeed widens the dynamic range for the static scene. However, it suffers from ghost artifacts caused by moving objects and/or moving camera while capturing the scene, and thus needs complicated post-processing to remove the ghosts [23–26]. On the other hand, the space-division multiplexing methods using multiple sensors do not have ghost artifact problem, but they need complicated registration and interpolation process to match the view differences between the sensors [27]. The single image HDR is to mimic this process, i.e., it generates pseudo multi-exposure images from a single input image and then follows the original HDR imaging method for producing HDR images or tone-mapped-like exposure-fusion images for the LDR display.

In this paper, we propose a new singe image HDR imaging method based on the Retinex filtering scheme, mainly for the purpose of image enhancement under the undesirable illumination conditions. The proposed algorithm first decomposes an input image into illumination and reflectance component by using an edge-preserving smoothing filter. Then, the reflectance component is scaled to improve the details in relatively bright areas. Also, we devise an algorithm that

appropriately scales up and down the illumination component, in order to generate several illumination images that correspond to certain camera exposure values different from the original. The conventional exposure fusion method is applied to these illuminations to produce an equalized illumination. Then the enhanced reflectance is multiplied with the equalized illumination to produce the final enhanced image. In this process, we also propose a method to generate appropriate weight maps for keeping the contrast.

The rest of his paper is organized as follows. The overview of related works is presented in Section II. In Section III, the proposed illumination equalization method is discussed in detail. Experimental results and discussions are presented in Section IV. Finally, we draw our conclusions in Section V.

II. RELATED WORKS

The conventional methods for enhancing the undesirably illuminated images are the histogram equalization (HE) and its variants such as adaptive histogram equalization (AHE) [8], contrast limited adaptive histogram equalization (CLAHE) [10] and two-dimensional (2D) histogram approach in [28] named as contextual and variational contrast (CVC) enhancement. Another approach is the single scale Retiex (SSR) image enhancement method [17], which finds the illumination-compensated result from the functional forms of center/surround Retinex. Specifically, the average intensity in the surround of a pixel corresponds to the illumination and thus dividing this value from the original corresponds to the illumination-compensated pixel value. However, due to the difficulty in selecting the scale parameter, multi-scale Retinex (MSR) that decides the output image by a weighted sum of SSR outputs with different scales is also developed, and multi-scale retinex with color restoration (MSRCR) was also proposed to remove the artifacts that appear in MSR algorithm [18, 19].

Instead of histogram-based or Retinex filtering methods, a more intuitive approach to solving the illumination problem may be to appropriately adjust the illumination component, because the HVS is more sensitive to the illumination changes than the color variations. There are illumination adjustment methods based on this principle [5–7], and it is shown that they have the advantage of preserving the naturalness while unveiling the details in dark shadow areas. More precisely, Wang et. al. [6] proposed a naturalness preserving enhancement algorithm (NPEA) for improving the non-uniformly illuminated images. Based on the Retinex approach, an input image is decomposed into reflectance and illumination component by using a bright-pass filter. Then the estimated illumination component is adjusted by a bi-log transformation, while trying to preserve the naturalness by observing the measure of lightness-order error. In the case of low-light image enhancement (LIME) method proposed in [7], they mainly focused on the exact estimation of illumination component. In detail, initial illumination of each pixel is estimated by individually finding the maximum values in three color channels (Red, Green and Blue). Then, a structure-aware smoothing model that is developed to refine the initial illumination component

Fig. 1: A non-uniformly illuminated image and its illumination equalized result: (clockwise from top left) an input image 'Lighthouse,' estimated illumination, equalized illumination by adding the pseudo multi-exposure illuminations, and enhanced image using the equalized illumination.

is applied to obtain the sophisticated illumination. For the reflectance component, a denoising technique is employed to suppress possible noise in dark areas. Finally, they reproduced an improved image by combining the adjusted illumination and the denoised reflectance. In fusion-based image enhancement method (FbEM) [5], they first estimated the illumination component of input image by using the brightest channel prior, which is inspired from the dark channel prior (DCP) used for the dehazing algorithms [29]. Then, two different versions of illuminations, luminance-improved and contrast-enhanced illumination components, are derived by using an adaptive histogram equalization and a sigmoid function. Then the appropriate weights are designed for these illumination components, and the weighted illuminations are blended to be a final bright and contrast enhanced illumination. Finally, they reproduced an improved image by combining the adjusted illumination with the reflectance.

III. PROPOSED ENHANCEMENT ALGORITHM

A. Motivation and Overview

The dynamic range of most commercial cameras is limited so that they have problem with wide dynamic range scenes or with the very low light conditions. Specifically, the images often lose details in some regions when they are taken under undesirable illumination conditions such as backlight, non-uniform light or extremely low light environment. In this paper, we attempt to enhance such images based on the Retinex filtering, i.e., we estimate illumination and reflectance of the image and process them separately.

In general, it is difficult to obtain the accurate illumination by using the conventional filter-based estimation methods. Since the illumination is estimated as the weighted average of neighboring pixels, it is affected by the reflectance and thus does not appear uniform even in uniformly illuminated areas as shown in Fig. 1. The top-left figure is the input image, where the shore area is supposed to have uniform

Input Image

S

RGB-Luminance
Conversion

L

Decomposition
(Retinex/ WLSF)

R | I

Selective
Reflectance
Scaling

Virtual
Illumination
Generation

R' | $\{I_k\}$

Luminance
Reproduction

Weight Map
Generation

$\{L_k\}$ | $\{w_k\}$

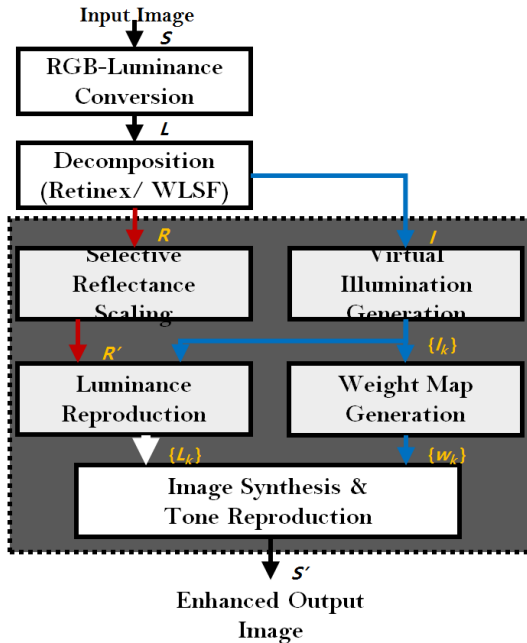Image Synthesis &
Tone Reproduction

S'

Enhanced Output
Image

Fig. 2: Block diagram of the proposed method.

illumination change. However, the estimate of illumination (top-right figure) in this area does not appear uniform because it is affected by the reflectance values of ocean and sand. Hence we attempt to obtain more equalized illumination via the fusion of pseudo multi-exposure illuminations as shown in the bottom-right figure, and multiply it with the reflectance to obtain the equalized output in the bottom-left of Fig. 1.

Our algorithm is basically based on the single HDR approach. By increasing and decreasing the illumination to several levels, we generate several illumination images which correspond to different camera exposure values. Multiplication of these illuminations to the reflectance produces pseudo multi-exposure images, and then we can finally obtain the enhanced image by using a multi-exposures fusion algorithm.

In summary, our contribution is to design a simple and effective method for enhancing the estimated reflectance and illumination, and also to further enhance the overall image by generating pseudo multi-exposure illuminations and combining them in the manner of exposure fusion. The most important and sophisticated process in our algorithm is to generate multiple illuminations that correspond to the multiple LDR images of different exposures for HDR imaging, without any prior information (capture device, exposure conditions etc.) on the input images.

The block diagram of our method is depicted in Fig. 2 and the contributions are indicated in the dark gray box. The proposed algorithm is consisted of three steps. The first step is to extract the luminance information (L) from an input RGB image (S) by the RGB to Lab transform, and then to decompose L into illumination (I) and reflectance component (R). We employ the weighted least square filter (WLSF) instead of Gaussian filter that is frequently used in the conventional methods in order to prevent the halo artifacts. The second step is to adjust the reflectance and illumination component, and

then to generate virtual illuminations that correspond to several different exposure values. For the adjustment of reflectance, we propose a selective reflectance scaling (SRS) method which enhances the details in relatively bright areas, which contributes to contrast enhancement. Simultaneously, we equalize the illumination and then generate several illuminations by developing a virtual illumination generation (VIG) method. Specifically, our VIG generates a set of multiple illuminations $(\{I_k\})$ which correspond to the ones in multi-exposure HDR imaging techniques. Then, a set of new luminance images $(\{L_k\})$ is reconstructed by combining the detail-improved reflectance (R') and the set of illumination components $(\{I_k\})$. We also design appropriate weights $(\{w_k\})$ that contribute to preserve the image details and to enhance brightness in every image area. Finally, the luminance images are fused to generate an enhanced one. By adopting tone reproduction process for the final luminance image, we obtain a brightness and detail-enhanced image.

B. Image Decomposition

The proposed enhancement algorithm starts with the Retinex-based illumination and reflectance decomposition. The luminance is first obtained from the input RGB image, and the reflectance information is obtained by the difference between the input luminance and the estimated illumination as

$$R(i,j) = log(L(i,j)) - log(I(i,j)) \quad (1)$$

where (i,j) is the index for pixel position, R corresponds to the reflectance information, L is the luminance, and $I = (L * G(\cdot))$ is the estimate of illumination obtained by the filtering of L with a filter G which is usually a normalized Gaussian function in the conventional works. However, it was reported that the Gaussian kernel generally makes halo artifacts near the border of bright background and dark foreground [30]. In general, the Gaussian filter needs a very large support such that the illumination estimation is less affected by reflectance values. However, this produces wrong estimates around the strong edges, which results in halo artifacts. Hence, we adopt the weighted least square filter (WLSF) instead of Gaussian to reduce the halo artifacts. The WLSF is a kind of edge-preserving and smoothing filters, where the filtering result is obtained by minimizing the following energy function:

$$E = \sum_p \left((u_p - L_p)^2 + \right.$$
$$\left. \lambda \left(a_{x,p}(L) \left(\frac{\partial u}{\partial x} \right)_p^2 + a_{y,p}(L) \left(\frac{\partial u}{\partial y} \right)_p^2 \right) \right) \quad (2)$$

where u is the output of the filtering, λ is the balancing parameter between the first and the second terms, and the subscript p denotes the pixel position. In the above energy function, the first term $(u_p - L_p)^2$ is to prevent the output u from being too much deviated from the input L, and the second is a smoothness term that suppresses textures by minimizing the partial derivatives $(\partial u)/(\partial x)_p$ and $(\partial u)/(\partial y)_p$. They can be further strengthened or weakened according to the strength

Fig. 3: Image decomposition: (clockwise from top left) an LDR input image of single exposure, estimated illumination component (corresponding to BM), inverse of BM (corresponding to DM) and reflectance component (adjusted for visualization).

of input texture by defining the weights $a_{x,p}(L)$ and $a_{y,p}(L)$ as

$$a_{x,p}(L) = \left(\left|\frac{\partial l}{\partial x}(p)\right|^{\alpha} + \epsilon\right)^{-1}$$
$$a_{y,p}(L) = \left(\left|\frac{\partial l}{\partial y}(p)\right|^{\alpha} + \epsilon\right)^{-1} \quad (3)$$

where the α is a control parameter for the sensitivity to the gradients of input L, and l is the log-luminance defined as $l = log(L + \epsilon)$ with a very small constant ϵ to prevent division by zero. The output of this WLSF is used as our initial illumination component (I).

However, like any other filter based estimation methods, the WLSF also underestimates the illumination in dark shadow areas or dark colored objects and thus the estimated illumination appears very small in such areas. Considering that increasing the brightness and contrast of dark areas is the basics of many image enhancement and HDR imaging techniques, we also increase the illumination in dark areas as long as the color is not too much distorted. In this process, the illumination in bright areas should not be affected too much, and thus we propose to adjust the illuminations of bright and dark areas separately. For this locally different adjustment strategy, we define two maps that represent the brightness/darkness of the illumination intensities. Specifically, the first map is named as the brightness map (BM) which is the image of normalized illumination intensity, and the second is the darkness map (DM) which contains the inverse of illumination at each pixel position. As an example, Fig. 3 shows an input image, BM, DM and reflectance components. We control the illumination changes considering these two intensity maps, which will be explained in Section III-D.

C. Selective Reflectance Scaling (SRS)

For enhancing the details in dark areas, illumination is going to be adjusted as will be described in the next subsection. However, in the case of bright areas, increasing the illumination may saturate the pixel values. Also, sharpness or details cannot be sufficiently enhanced in relatively well-illuminated
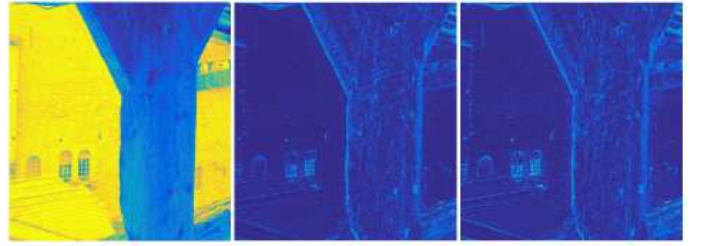

Fig. 4: Scaling the reflectance component by SRS: (from left to right) a cropped area of the image shown in Fig. 3, original reflectance of this area, and the enhanced reflectance, all represented in false color (blue: dark, yellow: bright).

areas since our illumination equalization method is not pixel-wise processing. For these reasons, instead of adjusting the illumination, we stretch the reflectance at bright areas where the illumination component is larger than a certain threshold. Precisely, the reflectance is modified according to

$$R'(i,j) = \begin{cases} R(i,j) \left(\frac{I(i,j)}{m_I}\right)^{\gamma_R}, & I(i,j) > m_I \\ R(i,j), & \text{otherwise} \end{cases} \quad (4)$$

where m_I is the average value of the estimated illumination and the parameter γ_R is the gamma value which is set to 0.5 in this paper. Hence when the illumination of a pixel $I(i,j)$ is larger than the mean m_I, then it is considered a bright pixel and the reflectance is increased by the amount of $\sqrt{I(i,j)/m_I}$. As a result, the details in bright areas become clearer than before. As an example, Fig. 4 shows the effect of the proposed algorithm. The first image is a crop of the image in Fig. 3, where the illumination of the pixels is shown in false color representation from yellow (bright) to blue (dark). The second is the reflectance value also in false color representation and the third is the result of applying our SRS in eq. 4. It can be observed that the texture (especially at the bright background) becomes apparent as a result of SRS. To validate the effect of SRS objectively, the 'discrete entropy (DE)' [31] is measured for the second and third images in Fig. 3, resulting in 2.30 and 2.42 respectively. The DE is devised to measure the total amount of information in the image and thus we can say that more information is unveiled by the SRS. The reason why we do not apply our SRS algorithm to dark areas is that it can amplify the noise in dark areas. Too much increase of brightness in dark areas can also reduce the overall contrast, which often makes the image seem unnatural. Hence the dark areas are improved by the illumination fusion method as follows.

D. Virtual Illumination Generation (VIG)

With a single input luminance L with unknown exposure value (EV), we design a simple and effective algorithm that generates multiple virtual illuminations. Specifically, we design a "scale function" that outputs a scale factor for the given virtual EV. Then the scale factor is multiplied to L to brighten or darken the original illumination according to the given EV.

For this, we first observe the illumination change in a set of real multi-exposure images acquired by 'bracketing.'

Fig. 5: Muli-exposure images and the relationship between the estimated illuminations: (top) under-, standard- and over-exposure LDR images of the 'Grandcanal' with exposure times of 1/750, 1/180 and 1/45, (bottom left) ratio of illumination of standard-exposure image to that of under-exposure image, (bottom right) ratio of illumination of over-exposure image to that of under-exposure image.

Specifically, consider a set of multi-exposure LDR images shown in Fig. 5 (top three), which are under-, standard- and over-exposure ones from left to right [32]. We denote the images as S_u, S_s and S_o and their illuminations I_u, I_s and I_o respectively. To investigate the tendency of illumination changes for these images, the ratios of illuminations are also shown in Fig. 5. The bottom-left image shows the ratio of standard-exposure to under-exposure, i.e, (I_s/I_u), and the bottom-right is the ratio of over-exposure to under-exposure (I_o/I_u). The figures clearly show that the ratio in shadow area is much larger than that in bright area. We take this observation into consideration, i.e., we adjust the illumination more in the dark regions than in the bright areas.

Also, we need to consider another aspect of camera imaging system that the scene radiance is nonlinearly mapped to the pixel values according to the sensor properties and other camera electronics. A global illumination adjustment method considering this property was proposed in [33], by designing a function that finds a global scale factor for the given EV. However, we do not take this approach because we consider more general case without EV information, and also because we are locally adjusting the illumination. Since we do not have EV for the given input, we instead define *virtual exposure value* (vEV), which is the average of normalized illumination in the range of [0,1]. We devise a function that maps a vEV to a scale factor, where the range of scale factor is adjusted according to the overall illumination. The illumination is globally adjusted according to the scale factor, and then locally adjusted depending on the local brightness.
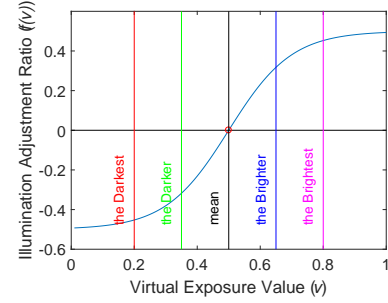
Our scale function is in the form of sigmoid, which has been commonly used for the tone-mapping and/or illumination compensation in the conventional works. Specifically, it is defined as

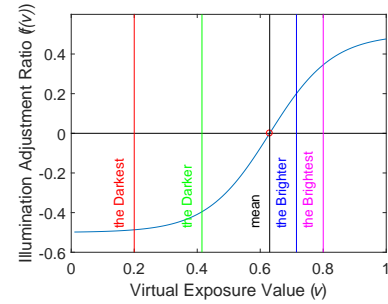$$f(v) = r\left(\frac{1}{1 + e^{-\sigma_s(v - m_I)}} - \frac{1}{2}\right) \quad (5)$$

where v is the vEV in the range of [0,1], m_I is the average of the normalized illumination of original image, σ_s is the
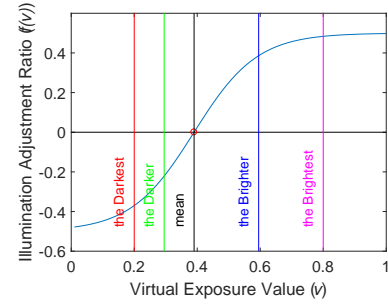
Fig. 6: The scale function for illumination adjustment. Examples for three cases are shown, (a) for relatively small average value $m_I < 0.5$, (b) for $m_I = 0.5$ and (c) for relatively large average value $m_I > 0.5$. Four different vEVs (from darkest to brightest) are indicated in each graph for generating four different virtual illuminations.

smoothness factor of the sigmoid curve which is just set to 1 in all of our experiments, and r is the adaptive amplitude which controls the range of the scale function. Fig. 6 shows some examples of this function for the cases of $m_I < 0.5$ (original image is rather dark on average), $m_I = 0.5$ (well-balanced input image), and $m_I > 0.5$ (bright image in overall region). It can be seen that the inflection point is set to m_I and the value of the function is 0 at this point. We can also see that the range of the function is larger when m_I is small in order to scale the illumination more for the darker images. The range of the function is controlled by r, which needs to be large when m_I is small and vice versa. This range control is easily implemented by defining it as

$$r = \left(1 - \frac{m_I}{M}\right). \quad (6)$$

where M is the maximum value of the illumination.

In the experiments, we generate four different illuminations that correspond to different vEVs, so that we have five illuminations including the original (vEV= m_I). Specifically, we define five v_k ($k = 1, 2, 3, 4, 5$) where $v_3 = m_I$, $v_1 = 0.2$, $v_5 = 0.8$, $v2 = (v_1 + v_2)/2$, and $v4 = (v_3 + v_5)/2$ as illustrated in Fig. 6b. In the figure, it can be seen that v_1 to v_5 correspond to the darkest, darker, original, brighter, brightest images. If m_I is less than 0.2 or larger than 0.8, then it means that most part of original image is saturated and thus we give up the enhancement. In all the experiments, there was actually no case that m_I is out of this range.

The global adjustment is to multiply $f(v_k)$ to the original illumination and add it to the original, i.e.,

$$I_k(i, j) = (1 + f(v_k))I(i, j). \tag{7}$$

As stated previously, we add local adjustment to the above equation for boosting the illumination change at dark areas. This is implemented as

$$I_k(i, j) = (1 + f(v_k))(I(i, j) + f(v_k)\breve{I}(i, j)) \tag{8}$$

where $\breve{I}$ is the inverse of the normalized initial illumination I, i.e., DM which is defined in Section III-B and shown in Fig. 3. Since the DM is large at the dark areas, the eq. 8 can enlarge the change of illumination more than the eq. 7 at the dark areas.

E. Tone Reproduction

The next step is to generate pseudo multi-exposure luminances from the enhanced reflectance R' and the I_k. For this we first obtain the luminance image for each vEV as:

$$L_k(i, j) = \exp(R'(i, j))I_k(i, j). \tag{9}$$

The generated luminance images are shown in Fig.7 for three vEVs. The first row shows the normalized illumination I_k for $k = 1, 3, 5$, and the second row shows the corresponding luminance images L_k. Additionally, differently illuminated RGB images S_k are shown in the third row. The S_k is obtained by using a conventional tone reproduction method [34]:

$$S_k = \begin{bmatrix} Red' \\ Green' \\ Blue' \end{bmatrix}_k = \begin{bmatrix} L_k \left(\frac{Red}{L}\right)^{\gamma_t} \\ L_k \left(\frac{Green}{L}\right)^{\gamma_t} \\ L_k \left(\frac{Blue}{L}\right)^{\gamma_t} \end{bmatrix} \tag{10}$$

where γ_t denotes the gamma correction coefficient in the range of [0,1]. In this paper, γ_t is just set to 1. As shown in the third rows in each image set in Fig. 7, they appear similar to multi-exposure LDR images obtained by bracketing.

F. Weight Rules for Luminance Synthesis

To blend the pseudo multi-exposure luminances as an illumination-equalized single luminance, we design an appropriate weighting rule which focuses on unveiling the details in dark areas and simultaneously maximizing the overall contrast. For this, the bright areas need to be stretched in the case of under-exposed images and conversely dark areas be stretched in the case of over-exposed ones. Precisely, for the under-exposed image, we take all the details in the brightest areas

(b)

Fig. 7: Generated virtual illuminations (L_k) and tone-reproduced images (S_k) from the virtual illuminations (I_k). The first row shows I_k, the second row L_k and the third S_k for $k = 1, 3, 5$ for the images of (a) Grandcanal and (b) Mask.

by setting the weights in these areas larger than others. This is simply implemented by setting the weight map as the normalized illumination values. Conversely, for the over-exposed luminance image, we take the details in the dark areas. Hence, we let the weighting values in the dark area be larger than those in other regions. This is achieved by setting the weight map as the inverse of normalized illumination. In summary, the weight maps are represented as

$$w_k = \begin{cases} \bar{I}_k, & k=1, 2, 3. \\ \bar{I}_k^{-1}, & k=4, 5. \end{cases} \tag{11}$$

where $\bar{I}_k$ is the normalized illumination, and $\bar{I}_k^{-1}$ means that each value in the illumination is inversed. The illumination images, luminance, and their weight maps are visualized in Fig. 8. There are two advantages in our weighting strategy. First, since the estimated illuminations (I_k) inherit the contrast of the input, the weight maps and the adjusted illuminations approximately succeed the image contrast. Second, our weight map is simple to obtain compared to the ones in the conventional exposure fusion methods [22, 23], which
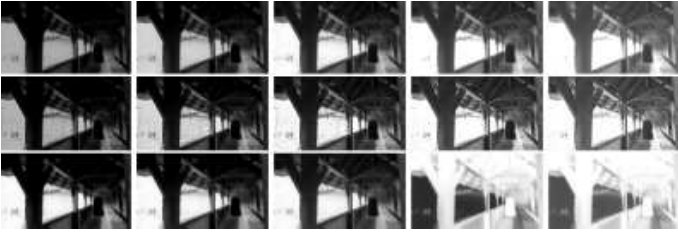
Fig. 8: Weight maps of differently exposed luminance images. First row: pseudo illuminations I_k, $k = 1, 2, \cdots, 5$. Second row: reproduced luminance images L_k. Third: weight maps w_k.

need complicated measures such as contrast, saturation and exposedness of pixels and/or regions.

Finally, we can obtain an illumination-equalized luminance by applying the conventional weighted-averaging as

$$L'(i,j) = \frac{\sum_{k=1}^{N} L_k(i,j) w_k(i,j)}{\sum_{k=1}^{N} w_k(i,j)}, \qquad (12)$$

where L' represents the final luminance image and w_k is the blending weight map for the k-th luminance image. The final enhanced image in RGB color space can be also obtained by using the eq. 10 with the final luminance image and color information of the original image.

IV. EXPERIMENTS AND DISCUSSIONS

Experiments are performed with the images from the other papers and MMSPG dataset [35] which are captured in various illumination conditions such as backlight, low light and non-uniform light environments.

A. Comparison with other methods

The proposed method is compared with the conventional histogram-based methods (CLAHE [10] and CVC [28]), a retinex-based algorithm (MSR) [18], and illumination adjustment methods such as NPEA, FbEM and LIME [5–7]. The parameters for these methods are set the same as the original work when they are clearly specified in the paper. Specifically, all the parameters for the CLAHE are set to be the default values. The parameters for CVC are set as $\alpha = 1/3$, $\gamma = 1/3$, and $\beta = 2$, and 7×7 block size is used. For MSR, the weights for three SSR results are set the same, and the patch sizes of three Gaussian functions are set to 15, 80, and 250 respectively. For NPEA, FbEM and LIME, the encrypted Matlab codes provided by the authors are used.

1) Subjective comparisons: First, the results for backlight images, which contain very bright and dark areas simultaneously, are presented in Figs. 9 and 10. As can be observed, CLAHE does not properly improve the brightness especially in the dark areas, and the CVC produces somewhat blurred and unnatural results. Although the MSR enhances details in dark areas clearly, there are some color distortions. On the other hand, the FbEM, LIME, NPEA and the proposed method show enhanced details in the shaded areas. In the case of LIME, however, it seems that the brightness is too much amplified.

Figs. 11 and 12 show the results for the images captured in the low light conditions. Similar to the backlight case, CLAHE and CVC fail to unveil the details in all areas. The MSR enhances details in all areas but the results look unnatural. The LIME over-enhances the image such that the results give the impression that the photo is taken at daytime while it was actually taken at dawn or night. The FbEM and the proposed algorithm generate similar result, but the proposed method shows more contrasted image and hence shows more vivid texture.

Results for the images taken under the non-uniform illumination condition are presented in Fig. 13. The non-uniform illumination means that there are low and highly illuminated regions within small areas. It is clear that the CLAHE generates a contrast-enhanced result, but it does not look natural as the texture on the duck becomes too dark. The CVC and MSR over-stretch the contrast and hence the results lose the details in bright areas. On the other hand, the FbEM, LIME, NPEA and the proposed method show quite pleasing results. Each result has its own pros and cons and the preference may be different from person to person. But, like the above cases, the LIME stretches bright areas too much such that the texture on the duck's feather is lost.

2) Objective comparisons: Since our HVS and its perception mechanism are so complicated, finding an objective image quality assessment (IQA) method that measures the degree of enhancement is very difficult. Actually, there may not be "objective" measure because the aesthetic perception is also individually different. Anyway, in this paper, we select two IQA metrics which have been adopted for similar purposes as our case. Specifically, we adopt the gradient magnitude similarity deviation (GMSD) as a full-reference IQA, and the natural image quality evaluator (NIQE) as a no-reference IQA method [36, 37]. The GMSD measures visual distortion between an input image and its enhancement [36]. The lower GMSD means less visual distortion. The NIQE is based on the statistical regularities that can be derived from natural and undistorted images[37]. The lower NIQE also means better quality. Table I lists these metrics for the images compared above, where the best and second best numbers are written in bold. While the proposed algorithm does not always show the best performance, it shows quite low values on average. Also, there are many cases that both of GMSD and NIQE measures are lower than others.

We carried out more experiments on 70 images from [6], and the average GMSD for NPEA/Ours is shown to be (0.118/0.065) and NIQE be (3.365/3.469). That is, our algorithm shows better results in terms of GMSD, and slightly worse in NIQE than the NPEA. However, as stated previously, the objective measure may not be in agreement with the individual's subjective assessment. As an example, Fig. 14 shows some results by NPEA and ours, where it seems that NIQE prefers stretching the brightness to keeping the naturalness or suppressing the distortions. For more subjective comparisons, refer to large images in our project page (https://github.com/JasonBournePark/EnhanceHDR), where materials for our algorithm are also available.

Fig. 9: Results for the image 'Wooden ceiling' labled as C23 in MMSPG dataset. From top left to bottom right: input image, result of CLAHE, CVC, MSR, FbEM, LIME, NPEA and proposed method.

Fig. 10: Results for the image 'Tile-roofed house' labled as C11 in MMSPG dataset. From top left to bottom right: input image, resu

Fig. 11: Results for the input image, 'Daybreak'. (from top left to bottom right) Input image, result of CLAHE, CVC, MSR, FbEM, LIME, NPEA and proposed method.

B. Discussions

1) Noise reduction: Generally, expanding the range of an image is accompanied by noise amplification especially in dark areas where the signal to noise ratio is inherently low. Hence our method (SRS) attempts to avoid the expansion of reflectance in dark areas, and instead increases the filtered illumination. Note that the illumination component is obtained by the WLSF that also reduces the noise. However the noise is still somewhat amplified, though less than the case of directly expanding the pixel values. For reducing the noise amplified by the enhancement, we may consider applying a noise reduction algorithm as a post-processing step. However, it should be noted that the noise reduction accompanies blurring effect, and filtering the reflectance component may result in large changes in the pixel values because the reflectance is described in log scale. Thus we apply the noise reduction to the illumination

component only, for keeping the edges and textures that are in the reflectance component.

As for the noise reduction, recent deep learning based methods [38, 39] perform better than the conventional transformation-filtering-based BM3D [40]. However, since the neural network methods need huge computing power (GPU) and also since the purpose of adopting the noise reduction in this paper is just to demonstrate an example of post-processing for further rectification, we just adopt the BM3D. Fig. 15 shows the result of this post-processing, where it can be seen that the noise is considerably reduced without any other side effect such as loss of details.

2) Detail enhancement on the reflectance: In this subsection, we discuss the effect of our reflectance manipulation (SRS in eq. 10) compared to the conventional methods that focus on increasing the illumination only. In Fig. 16, we

Fig. 12: Results for the input image, 'Entrance'. (from top left to bottom right) Input image, result of CLAHE, CVC, MSR, FbEM, LIME, NPEA and proposed method.

Fig. 13: Results for the input image, 'Duck'. (from top left to bottom right) Input image, result of CLAHE, CVC, MSR, FbEM, LIME, NPEA and proposed method.

Fig. 14: Sample images obtained by NPEA and the proposed method; (from left to right in each row) input images, output images by NPEA and ours.

Fig. 15: Noise reduction results, (from left to right in each row) input image, result of the proposed method and noise suppression result using BM3D.

TABLE I: GMSD and NIQE measurements.

Images	$CLAHE$		CVC		MSR		$FbEM$		$LIME$		$NPEA$		$OURS$	
	G	N	G	N	G	N	G	N	G	N	G	N	G	N
Tile-roofed house	0.134	1.572	**0.045**	1.746	0.289	1.940	0.105	**1.481**	0.189	1.708	0.117	1.557	**0.042**	**1.533**
Wooden ceiling	0.130	1.867	**0.022**	1.773	0.294	2.779	0.134	1.826	0.223	2.214	0.156	**1.526**	**0.079**	1.678
Daybreak	0.130	**3.183**	**0.069**	3.837	0.246	3.421	0.119	3.483	0.192	**3.382**	0.117	3.637	**0.088**	3.631
Duck	0.152	**2.651**	**0.121**	2.883	0.264	4.246	0.155	2.839	0.214	2.994	0.146	2.813	**0.082**	**2.488**
Entrance	0.148	3.441	0.209	3.264	0.264	3.780	**0.138**	3.524	0.221	3.582	0.174	**3.160**	0.132	**3.124**
Average	0.140	2.543	**0.093**	2.701	0.275	3.233	0.130	2.631	0.208	2.776	0.142	**2.539**	**0.085**	**2.491**

present the visual comparison again for another image, which is a kind of backlight and/or non-uniformly illuminated image. Since it has dark shadow and simultaneously bright areas, adjusting only the illumination does not improve the details in bright areas. In the CLAHE and MSR results, it can be observed that the details look considerably enhanced but the visual quality is degraded. In the result of CVC, only the brightness level is improved. The output image is over-enhanced in the case of LIME algorithm and hence details in bright areas become less visible. The FbEM and NPEA generate relatively well illuminated and comfortable images, but they did not much enhance the details in bright areas. In the case of proposed method, it appears that both of bright and dark areas are well enhanced.

3) Run-time comparison: Run-times are compared in Table II for several different resolutions. The proposed method requires relatively large run-time (denoted as w/ WLSF in the table) mainly due to the WLSF for generating the high quality edge-preserved illumination map [12]. The run-time without the WLSF (denoted as w/o WLSF) is much smaller than others. Hence, if we use a simple illumination estimation method such as global smoothing filter (GSF) [41], the run-time (denoted as w/ GSF) is less than others though there can be some degradation in image quality. Specifically, if we use GSF instead of WLSF, then the GMSD and NIQE measures increase approximately by 14% and 2% respectively.

C. HDR image generation and applications

1) Extension to the HDR reverse tone mapper: The main purpose of this paper is the image enhancement and so we have focused on evaluating our algorithm in comparison with other enhancement methods. In addition to this, since our method is basically a single image HDR, we briefly test it as an HDR imaging method.

Generating an HDR image from a single exposure image is called a single image HDR in some software tools or reverse tone mapping [21, 42–45]. The reverse tone mapping operation (rTMO) is an ill-posed problem because it tries to find the information that was lost during the capturing process. In this subsection, we test whether the pseudo multi-exposures generated by our algorithm can be used for generating an HDR image, i.e., we test the feasibility of our method for rTMO. For this, we generate some of the HDR images by the reverse tone mapping functions provided in the HDR Matlab toolbox [45] and also provided by the author in [21].

We set the parameters of our algorithm the same as in the image enhancement experiments above. The only additional processing is to generate an RGBE image (.hdr format) by encoding the enhanced luminance information (L') based on the target luminance range of a display. The parameters in each of compared rTMOs are set to be the default values, and the minimum and maximum luminance of target display are set to 0.0015 cd/m^2 (nits) and 3000 cd/m^2 respectively. The comparison is shown in Fig. 17, where the global tone-mapping function proposed in [46] is used for the LDR display. It can be seen that the proposed algorithm is comparable to the other conventional rTMOs.

2) Pre-processing and post-processing: We demonstrate that the proposed method is also suitable as a pre-processing step for the computer vision tasks. For example, we show that it is very effective for enhancing the objects in low illumination conditions such that it can enhance the performance of automatic number plate recognition (ANPR) system [51]. Specifically, the number plate in the left image of Fig. 18 is not detected, but after applying our algorithm we obtain the image as shown in the right side. Then we can successfully detect the plate and binarize it as shown in the bottom figures.

The proposed method can also be used as a post-processing step for further enhancing the images that are already processed for other purposes. For example, let us consider our method as a post-processor for haze removed images. Fig. 19 shows an input image with the haze (left), its enhancement by using the dark channel prior (DCP) method in [29] (center), and its enhancement by our algorithm (right). In general, the results of dehazing methods suffer from losing details and lack of brightness, and our algorithm can enhance the haze-removed images to be more visually pleasing.

V. CONCLUSION

We have proposed an image enhancement algorithm based on the single image HDR. The input image is first decomposed into reflectance and illumination components based on the Retinex theory. The reflectance image is separately manipulated to enhance the details in bright areas, and the illumination component is scaled up and down to generate several virtual illuminations that correspond to certain exposure values. That is, we generate several multi-exposure illuminations from the single input, and they are fused to be an enhanced illumination. Then we multiply the enhanced reflectance and fused illumination to obtain the final enhanced image. Experiments show that
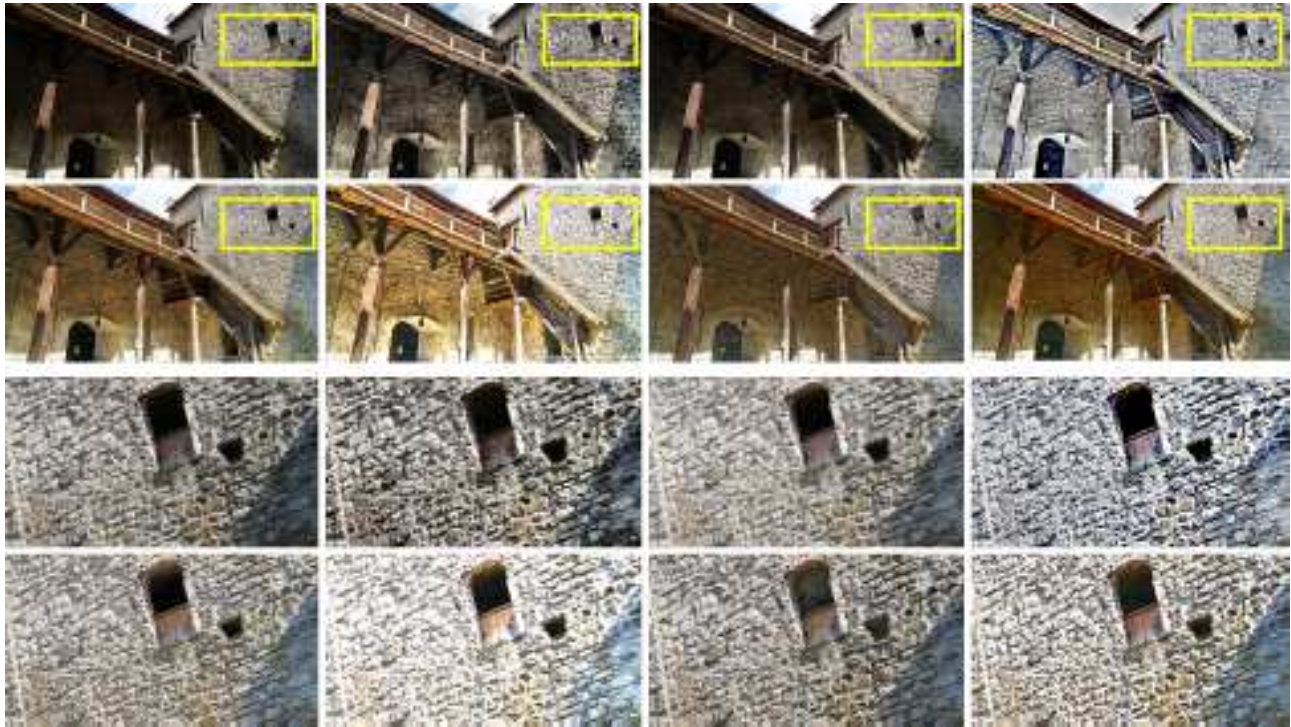
Fig. 16: Comparison of 'Stone wall' image labled as C25 in MMSPG dataset. From top left to bottom right: input image, CLAHE, CVC, MSR, FbEM, LIME, NPEA and the proposed. The third and fourth rows are the magnifications of yellow boxes

TABLE II: Run-time comparison.

Image resolution	$CLAHE$	CVC	MSR	$FbEM$	$LIME$	$NPEA$	$OURS$		
							w/o WLSF	w/ WLSF	w/ GSF
560×420	0.182	0.137	0.583	0.185	0.100	7.637	**0.084**	0.740	**0.095**
1038×789	1.055	0.565	1.749	1.928	1.046	27.065	**0.267**	2.537	**0.295**
1920×1080	1.344	1.205	3.020	1.416	0.955	68.181	**0.606**	6.987	**0.783**
1536×2048	2.054	2.027	4.557	2.141	1.571	103.755	**0.916**	12.684	**1.259**

the proposed method produces visually pleasing results, and also yields comparable or better results than the conventional methods in terms of some objective measures.

REFERENCES

[1] R. C. Gonzalez and R. E. Woods, "Image processing," *Digital image processing*, vol. 2, 2007.

[2] G. A. Baxes, *Digital image processing: principles and applications*. Wiley New York, 1994.

[3] C. Lee, C. Lee, and C.-S. Kim, "Contrast enhancement based on layered difference representation of 2d histograms," *IEEE Transactions on Image Processing*, vol. 22, no. 12, pp. 5372–5384, 2013.

[4] G. Deng, "A generalized unsharp masking algorithm," *IEEE transactions on Image Processing*, vol. 20, no. 5, pp. 1249–1261, 2011.

[5] X. Fu, D. Zeng, Y. Huang, Y. Liao, X. Ding, and J. Paisley, "A fusion-based enhancing method for weakly illuminated images," *Signal Processing*, vol. 129, pp. 82–96, 2016.

[6] S. Wang, J. Zheng, H.-M. Hu, and B. Li, "Naturalness preserved enhancement algorithm for non-uniform illumination images," *IEEE Transactions on Image Processing*, vol. 22, no. 9, pp. 3538–3548, 2013.

[7] X. Guo, Y. Li, and H. Ling, "Lime: Low-light image enhancement via illumination map estimation," *IEEE Transactions on Image Processing*, 2016.

[8] S. M. Pizer, E. P. Amburn, J. D. Austin, R. Cromartie, A. Geselowitz, T. Greer, B. ter Haar Romeny, J. B. Zimmerman, and K. Zuiderveld, "Adaptive histogram equalization and its variations," *Computer vision, graphics, and image processing*, vol. 39, no. 3, pp. 355–368,

Fig. 17: Tone mapped images of HDR images generated by several rTMOs. From top left to bottom right: input LDR image, Ak[...   ]9], Meylan et. al's [50], Rempel et. al's in [43], Wang et. al's [21] and[...]
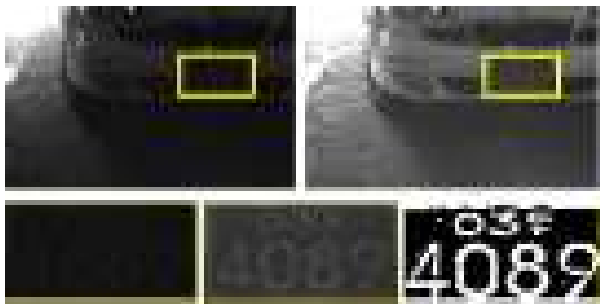

Fig. 18: Pre-processing for ANPR. Top left and right: input image and enhanced image by our proposed algorithm. Bottom, from left to right: enlargement of original, enhanced, binarized number plate.

1987.

[9] D.-I. Yoon, "Contrast enhancement using brightness preserving bi-histogram equalization," *School of Information and Computer Eng.*, 2008.

[10] E. D. Pisano, S. Zong, B. M. Hemminger, M. DeLuca, R. E. Johnston, K. Muller, M. P. Braeuning, and S. M. Pizer, "Contrast limited adaptive histogram equalization image processing to improve the detection of simulated spiculations in dense mammograms," *Journal of Digital imaging*, vol. 11, no. 4, pp. 193–200, 1998.

[11] T. Arici, S. Dikbas, and Y. Altunbasak, "A histogram modification framework and its application for image contrast enhancement," *IEEE Transactions on image processing*, vol. 18, no. 9, pp. 1921–1935, 2009.

[12] Z. Farbman, R. Fattal, D. Lischinski, and R. Szeliski, "Edge-preserving decompositions for multi-scale tone and detail manipulation," in *ACM Transactions on Graphics (TOG)*, vol. 27, no. 3. ACM, 2008, p. 67.

[13] E. P. Bennett and L. McMillan, "Video enhancement using per-pixel virtual exposures," in *ACM Transactions on Graphics (TOG)*, vol. 24, no. 3. ACM, 2005, pp. 845–852.

[14] F. Durand and J. Dorsey, "Fast bilateral filtering for the display of high-dynamic-range images," in *ACM transactions on graphics (TOG)*, vol. 21, no. 3. ACM, 2002, pp. 257–266.

[15] Y. Wang, S. Zhuo, D. Tao, J. Bu, and N. Li, "Automatic local exposure correction using bright channel prior for under-exposed images," *Signal Processing*, vol. 93, no. 11, pp. 3227–3238, 2013.

[16] E. Eisemann and F. Durand, "Flash photography enhancement via intrinsic relighting," *ACM transactions on graphics (TOG)*, vol. 23, no. 3, pp. 673–678, 2004.

[17] D. J. Jobson, Z.-u. Rahman, and G. A. Woodell, "Properties and performance of a center/surround retinex," *IEEE transactions on image processing*, vol. 6, no. 3, pp. 451–462, 1997.

[18] L. Meylan and S. Süsstrunk, "Color image enhancement using a retinex-based adaptive filter," in *Conference on Colour in Graphics, Imaging, and Vision*, vol. 2004, no. 1. Society for Imaging Science and Technology, 2004, pp. 359–363.

[19] R. Kimmel, M. Elad, D. Shaked, R. Keshet, and I. Sobel, "A variational framework for retinex," *International Journal of computer vision*, vol. 52, no. 1, pp. 7–23, 2003.

[20] C.-H. Lee, L.-H. Chen, and W.-K. Wang, "Image contrast enhancement using classified virtual exposure image fusion," *IEEE Transactions on Consumer Electronics*, vol. 58, no. 4, 2012.

[21] T.-H. Wang, C.-W. Chiu, W.-C. Wu, J.-W. Wang, C.-Y. Lin, C.-T. Chiu, and J.-J. Liou, "Pseudo-multiple-exposure-based tone fusion with local region adjustment," *IEEE Transactions on Multimedia*, vol. 17, no. 4, pp. 470–484, 2015.

[22] E. Reinhard, W. Heidrich, P. Debevec, S. Pattanaik, G. Ward, and K. Myszkowski, *High dynamic range imaging: acquisition, display, and image-based lighting.* Morgan Kaufmann, 2010.

[23] T. Mertens, J. Kautz, and F. Van Reeth, "Exposure fusion: A simple and practical alternative to high dynamic range photography," in *Computer Graphics Forum*, vol. 28,

Fig. 19: Post-processing of haze removed image. From left to right: input image, haze-removed image and enhanced image by our proposed algorithm.

no. 1. Wiley Online Library, 2009, pp. 161–171.

[24] J. An, S. H. Lee, J. G. Kuk, and N. I. Cho, "A multi-exposure image fusion algorithm without ghost effect," in *Acoustics, Speech and Signal Processing (ICASSP), 2011 IEEE International Conference on*. IEEE, 2011, pp. 1565–1568.

[25] J. An, S. J. Ha, and N. I. Cho, "Probabilistic motion pixel detection for the reduction of ghost artifacts in high dynamic range images from multiple exposures," vol. 2014, no. 1. EURASIP, 2014, pp. 1–15.

[26] J. An, S. J. Ha, and N. I. Cho, "Reduction of ghost effect in exposure fusion by detecting the ghost pixels in saturated and non-saturated regions," in *Acoustics, Speech and Signal Processing (ICASSP), 2012 IEEE International Conference on*. IEEE, 2012, pp. 1101–1104.

[27] S. K. Nayar and T. Mitsunaga, "High dynamic range imaging: Spatially varying pixel exposures," in *Computer Vision and Pattern Recognition, 2000. Proceedings. IEEE Conference on*, vol. 1. IEEE, 2000, pp. 472–479.

[28] T. Celik and T. Tjahjadi, "Contextual and variational contrast enhancement," *IEEE Transactions on Image Processing*, vol. 20, no. 12, pp. 3431–3441, 2011.

[29] K. He, J. Sun, and X. Tang, "Single image haze removal using dark channel prior," *IEEE transactions on pattern analysis and machine intelligence*, vol. 33, no. 12, pp. 2341–2353, 2011.

[30] E. Zhang, H. Yang, M. Xu *et al.*, "A novel tone mapping method for high dynamic range image by incorporating edge-preserving filter into method based on retinex," *Applied Mathematics & Information Sciences*, vol. 9, no. 1, pp. 411–417, 2015.

[31] D.-Y. Tsai, Y. Lee, and E. Matsuyama, "Information entropy measure for evaluation of image quality," *Journal of digital imaging*, vol. 21, no. 3, pp. 338–347, 2008.

[32] The photomatix website. [Online]. Available: https://www.hdrsoft.com/index.html/

[33] G. Messina, A. Castorina, S. Battiato, and A. Bosco, "Image quality improvement by adaptive exposure correction techniques," in *Multimedia and Expo, 2003. ICME'03. Proceedings. 2003 International Conference on*, vol. 1. IEEE, 2003, pp. I–549.

[34] K. Kim, J. Bae, and J. Kim, "Natural hdr image tone mapping based on retinex," *IEEE Transactions on Con-sumer Electronics*, vol. 57, no. 4, 2011.

[35] P. Korshunov, H. Nemoto, A. Skodras, and T. Ebrahimi, "Crowdsourcing-based evaluation of privacy in hdr images," in *SPIE Photonics Europe*. International Society for Optics and Photonics, 2014, pp. 913 802–913 802.

[36] W. Xue, L. Zhang, X. Mou, and A. C. Bovik, "Gradient magnitude similarity deviation: A highly efficient perceptual image quality index," *IEEE Transactions on Image Processing*, vol. 23, no. 2, pp. 684–695, 2014.

[37] A. Mittal, R. Soundararajan, and A. C. Bovik, "Making a 'completely blind' image quality analyzer," *IEEE Signal Processing Letters*, vol. 20, no. 3, pp. 209–212, 2013.

[38] K. Zhang, W. Zuo, Y. Chen, D. Meng, and L. Zhang, "Beyond a gaussian denoiser: Residual learning of deep cnn for image denoising," *IEEE Transactions on image Processing*, 2017.

[39] B. Ahn and N. I. Cho, "Block-matching convolutional neural network for image denoising," *arXiv preprint arXiv:1704.00524*, 2017.

[40] K. Dabov, A. Foi, V. Katkovnik, and K. Egiazarian, "Image denoising by sparse 3-d transform-domain collaborative filtering," *IEEE Transactions on image processing*, vol. 16, no. 8, pp. 2080–2095, 2007.

[41] D. Min, S. Choi, J. Lu, B. Ham, K. Sohn, and M. N. Do, "Fast global image smoothing based on weighted least squares," *IEEE Transactions on Image Processing*, vol. 23, no. 12, pp. 5638–5653, 2014.

[42] F. Banterle, P. Ledda, K. Debattista, and A. Chalmers, "Inverse tone mapping," in *Proceedings of the 4th international conference on Computer graphics and interactive techniques in Australasia and Southeast Asia*. ACM, 2006, pp. 349–356.

[43] A. G. Rempel, M. Trentacoste, H. Seetzen, H. D. Young, W. Heidrich, L. Whitehead, and G. Ward, "Ldr2hdr: on-the-fly reverse tone mapping of legacy video and photographs," in *ACM transactions on graphics (TOG)*, vol. 26, no. 3. ACM, 2007, p. 39.

[44] C.-R. Chen, C.-T. Chiu, and Y.-C. Chang, "Inverse tone mapping operator evaluation using blind image quality assessment," in *Asia–Pacific Sign. and Information Proc. Association Annual Summit and Conf., APSIPA Oct*, 2011.

[45] F. Banterle, A. Artusi, K. Debattista, and A. Chalmers, *Advanced high dynamic range imaging: theory and prac-*

tice.   CRC press, 2011.

[46] E. Reinhard, M. Stark, P. Shirley, and J. Ferwerda, "Photographic tone reproduction for digital images," *ACM transactions on graphics (TOG)*, vol. 21, no. 3, pp. 267–276, 2002.

[47] A. O. Akyüz, R. Fleming, B. E. Riecke, E. Reinhard, and H. H. Bülthoff, "Do hdr displays support ldr content?: a psychophysical evaluation," *ACM Transactions on Graphics (TOG)*, vol. 26, no. 3, p. 38, 2007.

[48] F. Banterle, P. Ledda, K. Debattista, and A. Chalmers, "Expanding low dynamic range videos for high dynamic range applications," in *Proceedings of the 24th Spring Conference on Computer Graphics*.   ACM, 2008, pp. 33–41.

[49] Y. Huo, F. Yang, and V. Brost, "Dodging and burning inspired inverse tone mapping algorithm," *J. Comput. Inf. Syst.*, vol. 9, no. 9, pp. 3461–3468, 2013.

[50] L. Meylan, S. Daly, and S. Süsstrunk, "The reproduction of specular highlights on high dynamic range displays," in *Color and Imaging Conference*, vol. 2006, no. 1. Society for Imaging Science and Technology, 2006, pp. 333–338.

[51] R. Lotufo, A. Morgan, and A. Johnson, "Automatic number-plate recognition," in *Image Analysis for Transport Applications, IEE Colloquium on*.   IET, 1990, pp. 6–1.